Quantification Analysis of Geometric Characteristics of Micro Crack Network On Fault Rock Surface

Haitao Yu
Southeast University

Zhibin Liu (seulzb@seu.edu.cn)
Institute of Geotechnical Engineering, School of Transportation, Southeast University
https://orcid.org/0000-0001-6602-1275

Yun Zhang
Guangxi Beitou Construction and Investment Group Co.， Ltd.

Tingyi Luo
Guangxi Beitou Construction and Investment Group Co.， Ltd.

Yasen Tang
Guangxi Beitou Construction and Investment Group Co.，Ltd.

Research Article

Keywords: Fault rock, Crack network, Geometry characteristics, Clay

Posted Date: January 3rd, 2022

DOI: https://doi.org/10.21203/rs.3.rs-1131339/v1

Abstract

Fault is a common water conduit in coal mine, and the cracks of fault rock will greatly affect its permeability. In this study, three fault samples obtained in the mining area in Southwest Shandong of China was tested and observed by SEM, XRD and plane-polarized light microscope. The geometric characteristics, including crack density, fractal dimension and crack connectivity, of the crack network on the sample surface were calculated. Combined with the mineral content obtained by XRD, the nonuniformity coefficient of mineral composition in rock is defined. The results show that the crack geometric characteristics of the three samples are quite different and the above geometric parameters of crack network on three fault rock samples are correlated. The optical photomicrographs and SEM images show that the crack network is developed most in the fault rock samples with the least clay content. The study suggests that the nonuniformity coefficient of rock samples is positively correlated with the geometric characteristic of crack network. The difference in the crack network of fault rock samples is related to the coefficient of friction of clay.

1. Introduction

Due to the complex geological environment of the fault zone, the fault rocks have high heterogeneity, which has an important impact on the macro mechanical properties and permeability properties of the rocks (Bense et al. 2013; Michie et al. 2021; Walker et al. 2013). The rock mass in the fault zone breaks under the action of structural stress, and there are a large number of cracks in the fault rock. The structural plane on the macro scale determines the permeability of the fault to a great extent (Bauer et al. 2016; Bense and Person 2006; Caine et al. 1996; Cooke et al. 2018). In addition, fault rock itself also has some microcracks (Kim et al. 2004). Although these microcracks have little effect on permeability, these defects tend to expand (Liang et al. 2012; Liu et al. 2016), especially under the disturbance of manual excavation, such as coal mine excavation (Donnelly 2006).

As water conduits, the study of microcracks is very important to assess the permeability of fault rock. The connectivity of crack network is an important parameter in the permeability estimation model of fault rock. There are many descriptions about the concept of connectivity. Most of these definitions are based on the intersection of cracks (Kushch et al. 2009; Robinson 1983; Zhou et al. 2011). Topology, which also pays attention to the attributes of network nodes, has also been widely used in the research of crack networks in recent years, and shows very good advantages (Lahiri 2021; Li et al. 2020; Sanderson and Nixon 2018; Valera et al. 2018). In addition, fractal characteristics can also be used as an index to describe the complexity of crack network. Generally speaking, the more complex the crack network of rocks, the higher the fragmentation degree of rocks, which is beneficial to seepage (Jafari and Babadagli 2012; Miao et al. 2015).

Many synthetic random crack network models are established, such as continuous medium model, discrete medium model, percolation model and so on. These models reveal the relationship between the geometric characteristics of crack network and macro properties of rock from different angles (de Dreuzy

et al. 2001; Jiao et al. 2018; Mourzenko et al. 2011). Different from synthetic crack networks, natural crack networks are often more complex and difficult to predict. In order to accurately detect and describe rock cracks, new technologies are constantly applied. In addition to conventional acoustic positioning methods, in order to more intuitively observe the morphological characteristics of cracks, imaging technologies such as scanning electron microscope and X-ray CT are also widely used in rock crack observation, which can provide two-dimensional or three-dimensional images in micron level (Litorowicz 2006; Mac et al. 2021).

At present, there are many researches on the crack network of isotropic rock, including natural joints and prefabricated cracks of rock samples, which is helpful to understand the damage mechanism and failure behavior of rock. Nevertheless, there are few studies on the failure and damage of crack network of anisotropic natural rock. In the present study, the geometric characteristics of crack network on fault rock sample from Shandong, China are studied by sections, and the failure mechanism of fault rock is discussed.

2. Materials And Methods

2.1 Fault samples

As shown in Fig. 1, the study area is located in a mining area in the southwest of Shandong Province, China. The overall geological structure in the area is mainly composed of 70 faults, with a density of 11/km^2. The area is dominated by large and medium-sized faults with large drop and long extension. In order to master the specific conditions of large faults in the mining area, geological exploration holes were designed and the fault zone was exposed at the depth of 673.73m-739.12m. The normal fault with a drop of 120-140m is located in the upper part of Shanxi formation. The borehole revealed that the fault length of this section is 65.39m, the core length is 51.30m, and the core recovery is 78.45%. The core color is mainly grayish black and grayish white. The lithology is mainly sandy mudstone, medium sandstone and siltstone. Locally, it contains plant debris fossils and calcite veins. The core at the depth of 689.12m-701.32m (mainly medium sandstone, including a small amount of siltstone and mudstone) is relatively complete. The core at the depth of 701.32m-712.74m is mudstone containing plant clastic fossils and a large amount of argillaceous locally, which is close to coal seam. Below the coal seam is siltstone with cracks. The fault core in this section has the characteristics of “fracture-intact-fracture”. In addition, there are great differences in the degree of fragmentation and weathering in different layers. Therefore, the fault core is divided into upper, middle and lower sections according to the sample characteristics and depth.

2.2 Test methods and geometric characteristic parameters

In this study, the crack morphology of fault samples was observed by plane-polarized light microscope and scanning electron microscope. Under certain pressure and temperature conditions, the blue epoxy resin is pressed into the rock. After it is cured, the cast sheet is polished, and then placed under the plane-polarized light microscope for observation. The microstructure of fault rocks was observed by Scanning

Electron Microscope - Back-scatter Electron (SEM-BSE) microscopy. The phase composition is detected by XRD. After the fault samples are tested, the diffraction results are analyzed by using the standard comparison card in Jade analysis software to obtain the X-ray diffraction analysis patterns of each sample and conduct semi quantitative analysis (Nikkhah et al. 2017).

In order to analyze the geometric characteristics of cracks in fault rocks, the optical photomicrographs are imported into the Auto CAD. The cracks that can be distinguished and recognized are identified by using polylines, and a digital generalized crack network is obtained for geometric characteristics analysis.

The research on the crack characteristics can be divided into single crack and crack network. The connectivity degree of each crack has a significant impact on the permeability of the fault. The study of single crack mainly focuses on the length, opening and roughness of crack, while the study of crack network focuses on its geometric characteristic parameters. The characterization indexes of rock crack network include crack density, connectivity, fractal characteristics of crack network and so on.

Crack density

In the study of crack density, there are many different definitions of crack density. Litorowicz (2006) defined the crack density as the ratio of the total length of cracks in each image to the image area when studying cracks in concrete structures. Leung and Zimmerman (2012) defined crack density as the total number of cracks per unit area in the study of estimating hydraulic conductivity by statistical parameters of random crack network. In the effective medium theory, cracks are usually regarded as inclusions in porous materials. The crack density is usually expressed as dimensionless area density (Bristow 1960). In this paper, the crack density is calculated by this dimensionless method:

$$\rho = \frac{1}{A}\sum_{i=1}^{n}\left(\frac{l_i}{2}\right)^2$$

1

Where A is the area of the digitized image, which is 10.63 mm^2, n is the total number of cracks in image area, l_i is the length of cracks.

Fractal dimension

Fractal dimension is an important parameter to describe crack distribution. At present, the main method to calculate the fractal dimension is the grid covering method (Mandelbrot 1982). The natural cracks in rocks have certain self-similarity. F is a set of bounded points on the plane, which is contained in a rectangular region. The rectangular region is divided into smaller grid that side length is ε according to a certain proportion r. If the number of non-null grid is $N(r)$, the capacity dimension D_c is defined:

$$D_c = -\lim_{r\to 0}\frac{\ln N(r)}{\ln r}$$

2

Crack connectivity

The topological property of crack network means that the connection structure of each crack will not change due to the change of crack length and node position. This research method for crack connectivity can avoid the influence of scale effect, because topology pays more attention to the inherent properties of crack network (Valentini et al. 2007).

According to the topological graph theory, any crack network is composed of nodes and segments. Nodes are the points where two crack intersect or pinch out, and segments are the crack connecting two nodes. As shown in Fig. 2, nodes can be divided into X-type nodes (cross), Y-type nodes (adjacent) and I-type nodes(isolated) (Sanderson and Nixon 2018). The connectivity f of crack network can be calculated from the number of nodes of the above three types.

Saevik and Nixon (2017) compared five topological graphs used to describe the connectivity of crack network and obtained the expression of connectivity after fitting most suitable for predicting the hydraulic connectivity of variable topological crack mode:

$$\begin{cases} \eta = \dfrac{4n_X + 2n_Y}{4n_X + 2n_Y + n_I} \\ f = max(0, 2.94\eta - 2.13) \end{cases}$$

3

where η is the equivalent average connection number of each crack, f is the connectivity of crack network, n_X, n_Y an, n_I are the number of X-type nodes, Y-type nodes and I-type nodes.

Nonuniformity coefficient

(Ke et al. 2011) established a virtual internal bond model based on meso damage and simulated the dynamic process of crack generation and propagation in anisotropic rocks. The results show that the higher the uniformity coefficient is, the higher the macro mechanical strength is. Xia et al. (2021) defined the quantitative calculation method of nonuniformity coefficient based on normal distribution, which is the ratio of standard deviation of Young's modulus of rock to expectation. Because the fault rock also has nonuniformity of strength distribution and randomness of mineral distribution, the concept of nonuniformity coefficient is also applicable. However, the proportion of main minerals in rocks also has a great impact on the properties of rocks. Based on the research of Xia et al. (2021), the mineral content is increased and Equation 4 is proposed to describe the nonuniformity coefficient:

$$c = \frac{\max\left(E_i\omega_i\right) - \min\left(E_i\omega_i\right)}{\dfrac{\sum_{i=1}^{n} E_i\omega_i}{n}}$$

4

Where c is the nonuniformity coefficient; E_i is the Young's modulus of mineral, GPa; ω_i is the content of minerals in rock.

3. Results

According to the optical photomicrographs, the quartz particles in the upper sample are generally small, and there are large particles locally. Kaolinite is filled in the quartz, which is enriched locally. The cracks have similar strike (Fig. 3a). The clay mineral content of the middle section sample is low, partially filled with mineral veins, with a high degree of fragmentation, and the maximum width of the crack is about 0.06mm (Fig. 3b). The main mineral in the lower section of the sample is kaolinite. Because it is close to the coal seam, there is more black organic matter in the quartz (Fig. 3c).

The crack statistics on the surface of fault rock samples are shown in Fig. 3. There are 19 cracks on the surface selected on the fault sample with the depth of 681.1m-681.7m. The crack length ranges from 0.08mm-2.60mm, and the crack with the length less than 0.5mm accounts for 36.84% (Fig. 3a). The crack network on the surface of fault samples with depth of 701.6m-702.8m is developed, with a total of 121 cracks. The crack length ranges from 0.06mm-2.73mm. The cracks with a length less than 0.5mm account for 67.77%, accounting for the highest proportion, and the cracks greater than 1mm account for only 9.92%. There are only 7 cracks on the surface of fault samples with depth of 735.7m-737.3m, of which one through crack is 4.27mm long, and the rest are cracks less than 1mm. Generally, it is dominated by short and small cracks.

The calculated geometric parameters of crack network are shown in Table 1. The crack density of the middle section is 1.25, about three times that of the other two sections. The fractal results of three samples show that the average value of fractal dimension of crack in the middle section is 1.27 that is also the highest of the three samples. The fractal results show that the crack development degree of the fault sample in the middle section is the highest, the second is the upper sample and the lower sample is the lowest (Fig. 4).

Table 1
Geometric parameters of crack network of three segment fault rocks

Depth	n_X	n_Y	n_I	η	ρ	D_c
681.1m-681.7m	0	7	26	1.03	0.47	0.48-1.29
701.6m-702.8m	14	143	50	2.57	1.25	0.90-1.52
735.7m-737.3m	0	1	13	0.39	0.44	0.40-1.14

According to the results of scanning electron microscope (Fig. 5), many cracks and micro pores are developed on the surface of the fault rock. The crack length can reach hundreds of microns, and some cracks have been connected, and mineral particles can be seen in crack. There are many striae and a long

crack on the surface of the upper sample, the crack structural planes on both sides are uneven, and some cracks contain fine or coarse mineral particles. There are large black patches and small white mineral particles on the surface of the middle section sample. In addition, there are three connected cracks, which result in more microcracks. After 5000 times magnification, it is found that the crack structure is complex and the crack surface is rough. Only one crack is developed on the selected surface of the lower section of the sample. Most of other cracks are closed and the width of some cracks is about 5μm.

The results of XRD diffraction pattern interpret that all three samples contain quartz and kaolinite. Besides, the middle section samples also have muscovite, microcline and albite The difference is that the kaolinite content of the lower sample is the highest. Since the young's modulus of mineral particles is not tested in this study, in order to calculate the nonuniformity coefficient, the young's modulus of quartz, kaolinite, muscovite, microcline, albite tested in other studies are referred (Benazzouz and Zaoui 2012; Luu et al. 2021; Zhang et al. 2009). The young's modulus values used in this study are 105.6 GPa, 40.7 GPa and 74.4 GPa, 73.6 GPa, 86.0 GPa respectively. Then the nonuniformity coefficient can be calculated, as shown in Table 2.

Table 2 Mineral content and nonuniformity coefficient in each segment fault rock

Depth (m)	Mineral content					nonuniformity coefficient
	Quartz (%)	Kaolinite (%)	Muscovite (%)	Microcline (%)	Albite (%)	
681.1-681.7	85.9	14.1	-	-	-	1.76
701.6-702.8	40.8	7.5	28.5	14.3	8.8	2.34
735.7-737.3	38	62	-	-	-	0.47

4. Discussion

4.1 Correlation of geometric parameters of crack network

The optical photomicrographs and SEM images show the difference of crack development of the three fault rock samples. Taking crack density, connectivity and fractal dimension as quantitative indicators to describe the development degree, they all show as middle segment > upper segment > lower segment. The three parameters are dimensionless and have different research starting points. The calculation of crack density is based on the crack length. The connectivity is based on the topological properties of the network, and the type and number of crack intersections are concerned. The fractal dimension studies the self-similarity of crack network. Through comparison, it is found that the evaluation results of these three indicators are similar and have consistency (Fig. 7). Comparing the nonuniformity coefficient with the geometric characteristics of crack network, it is found that there is an obvious positive correlation

between them (Fig. 7). It indicates that the anisotropy of mineral composition has a great influence on the development of rock crack network.

The clay content and the geometric parameters of crack network are compared and analyzed. It indicates that the content of kaolinite in fault rocks is negatively correlated with the quantitative values of geometric parameters, as shown in Fig. 8. The SEM image shows that the crack width and connectivity of the upper and middle samples with higher content minerals such as quartz are higher than those of the lower fault samples with higher kaolinite content (Fig. 5). The analysis shows that kaolinite is easy to form filling, blocking and even closing at the pores and cracks due to its fine particle size. Kaolinite is a hydrophilic mineral with certain plasticity in case of water. It is easy to smear and fill the primary cracks, increasing the sealing of the fault rocks (Bense et al. 2013; Gui 2017).

4.2 Influence of clay content on crack network of fault rock

A large number of studies have confirmed the influence of clay minerals on fault weakening and sliding, because clay minerals have different coefficient of friction compared with other minerals. Similar to the geometric parameters of crack network, the coefficient of friction of fault rock and fault gouge often decreases with the increase of clay content (Fig. 9). The fracture form of the three samples in this paper accord with the three deformation mechanisms proposed by Lupini et al. (1981): (1) “turbulent mode”-when the clay content of is less than 25%, the sample is mainly brittle deformation of clastic particles in the shear deformation. (2) “sliding mode”-when the clay content is higher than 70%, the sample is mainly composed of clay with low friction strength, and the fracture is mainly due to the rotational arrangement of low friction clay particles along the shear surface (3) “transitional mode”- includes the above both turbulent and sliding shear. It can be seen from Table 2 that the upper and middle samples are “turbulent shear”, especially the middle samples. The whole is minerals with high friction strength such as quartz, and its stress support frame is debris support. The form of crack network indicates the brittle failure of this debris support under shear (Fig. 3b). The lower sample belongs to “transitional shear” but close to sliding shear, because the content of kaolinite is close to 70%. The relationship between coefficient of friction of and crack network still needs to be further studied.

Cracks mostly emerge and grow along the gap between quartz particles or clay filled between quartz particles. As shown in Fig. 10a, the distribution of quartz and other mineral particles in the fault rock samples has a relatively obvious boundary with the filling clay. The slender cracks mainly emerge in the clay, and the strike is along the filling clay. In Fig. 10b, there is no obvious boundary between the distribution of quartz particles and clay. Some short but unconnected fine cracks are distributed around the main cracks, which mainly develop in the parts of clay. If these short cracks are disturbed, they will have the trend of expansion and increase the fracture degree of rock. From the mechanical point of view, compared with mineral particles such as quartz and feldspar, clay such as kaolinite are the weak parts in fault rock. When subjected to shear action, the clay parts in fault rock are damaged first and further damaged with the increase of load. When the load reaches the failure strength of the developed quartz part, rock will produce brittle failure (Lan et al. 2010).

4.3 Prediction of equivalent permeability on crack networks

In previous studies, there have been a variety of prediction models for the equivalent permeability of crack networks (Lahiri 2021; Leung and Zimmerman 2012). However, due to the complexity of natural crack network, the available crack data are limited. The models in these studies have verified the accuracy of permeability estimation. It can be known that whether it is natural crack network or synthetic random crack network, the equivalent permeability in these estimation models is mainly composed of two parts. One is the attribute of a single crack in the crack network, which mainly focuses on the parameters such as crack length, crack width, crack surface roughness and crack dip angle. The other is the characteristics of crack network, such as connectivity, fractal dimension and so on. Based on this, this paper selects the equivalent permeability estimation model proposed by Sævik and Nixon, which considers the characteristics of crack network and each crack (Saevik and Nixon 2017):

$$K_{eff} = f \times \left(\frac{1}{A}\sum_{i=1}^{n} T_i L_i \boldsymbol{t}_i \, \boldsymbol{t}_i\right) \quad (5)$$

Where K_{eff} is the equivalent permeability. f is the crack connectivity. T_i, L_i and $\boldsymbol{t}_i$ is the transmittance, crack length and tangential vector of the crack respectively. T_i, L_i and $\boldsymbol{t}_i$ was not obtained in this study, only the contribution of crack connectivity to equivalent permeability is discussed here.

According to the prediction model (Eq. 3), the connectivity of the upper and lower fault samples is 0, and only the connectivity of the middle section is positive, which is 0.435. In other words, only the equivalent permeability of the middle section sample is positive, while the upper and lower section samples do not have permeability.

5. Conclusions

In this paper, the fault rock core exposed by geological exploration holes is divided into three sections, and the crack network characteristics of rock samples are studied. The main conclusions are given as follows.

(1) It is found that although the definitions of geometric parameters are different, these parameters are correlative in describing crack network on three fault rock samples. This result has reference significance for the parameter selection of equivalent permeability estimation model. Besides, according to the calculation results of the prediction model, only the middle section rock sample has equivalent permeability.

(2) The results indicate that the higher the nonuniformity coefficient of rock samples is, the higher the geometric characteristic parameters of crack network become. In addition, there is a negative correlation between the kaolinite content and the geometric parameters of the rock crack network. The tendency is similar to the coefficient of friction of fault rock. The discussion put up the view that the difference in the crack network of fault rock samples is related to the coefficient of friction of clay.

(3) The crack network is the most developed in the fault samples with the least clay content. The analysis shows that clay content is an important factor affecting the development of crack network on fault rock samples. Under the external force load, the clay mineral part in the rock probably first breaks and produces cracks.

Declarations

Acknowledgements:

The research was financially supported by the National Natural Science Foundation of China (No. 41877240, 41672280).

References

1. Bauer H, Schröckenfuchs TC, Decker K (2016) Hydrogeological properties of fault zones in a karstified carbonate aquifer (Northern Calcareous Alps, Austria). Hydrogeol J 24(5):1147–1170
2. Benazzouz BK, Zaoui A (2012) A nanoscale simulation study of the elastic behaviour in kaolinite clay under pressure. Mater Chem Phys 132(2–3):880–888
3. Bense VF, Gleeson T, Loveless SE, Bour O, Scibek J (2013) Fault zone hydrogeology. Earth-Sci Rev 127:171–192
4. Bense VF, Person MA (2006) Faults as conduit-barrier systems to fluid flow in siliciclastic sedimentary aquifers. Water Resour Res 42(W05421):1–18
5. Bristow J (1960) Microcracks, and the static and dynamic elastic constants of annealed and heavily cold-worked metals. Briti J Appl Phys 11(2):81–85
6. Caine JS, Evans JP, Forster CB (1996) Fault zone architecture and permeability structure. Geology 24(11):1025–1028
7. Cooke AP, Fisher QJ, Michie EAH, Yielding G (2018) Investigating the controls on fault rock distribution in normal faulted shallow burial limestones, Malta, and the implications for fluid flow. J Struct Geol 114:22–42
8. Crawford BR, Faulkner DR, Rutter EH (2008) Strength, porosity, and permeability development during hydrostatic and shear loading of synthetic quartz-clay fault gouge. J Geophys Res 113(B03207):1–14
9. de Dreuzy J-R, Davy P, Bour O (2001) Hydraulic properties of two-dimensional random fracture networks following a power law length distribution: 2. Permeability of networks based on lognormal distribution of apertures. Water Resour Res 37(8):2079–2095
10. Donnelly L (2006) A review of coal mining induced fault reactivation in Great Britain. Q J Eng Geol Hydroge 39(1):5–50
11. Gui H (2017) Impacts of Different Material Compositions on the Permeability of Fractured Fault Zone in Coal Measures. China University of mining and technology

12. Jafari A, Babadagli T (2012) Estimation of equivalent fracture network permeability using fractal and statistical network properties. J Petrol Sci Eng 92–93:110–123
13. Jiao C, Hu Y, Xu X, Lu X, Shen W, Hu X (2018) Study on the effects of fracture on permeability with pore-fracture network model. Energ Explor Exploit 36(6):1556–1565
14. Ke CR, Jiang JL, Ge XR, Xiao BL (2011) Numerical simulation on influence of heterogeneity on macroscopic fracture process of rock failure. Chin J Rock Mech Eng 30(S2):4093–4098
15. Kim Y-S, Peacock DC, Sanderson DJ (2004) Fault damage zones. J Struct Geol 26(3):503–517
16. Kushch V, Shmegera S, Sevostianov I (2009) SIF statistics in micro cracked solid: effect of crack density, orientation and clustering. Int J Eng Sci 47(2):192–208
17. Lahiri S (2021) Estimating effective permeability using connectivity and branch length distribution of fracture network. J Struct Geol 146(104314):1–19
18. Lan H, Martin CD, Hu B (2010) Effect of heterogeneity of brittle rock on micromechanical extensile behavior during compression loading. J Geophys Res 115(B01202):1–14
19. Leung CTO, Zimmerman RW (2012) Estimating the Hydraulic Conductivity of Two-Dimensional Fracture Networks Using Network Geometric Properties. Transport Porous Med 93(3):777–797
20. Li W, Zhao H, Wu H, Wang L, Sun W, Ling X (2020) A novel approach of two-dimensional representation of rock fracture network characterization and connectivity analysis. J Petrol Sci Eng 184(106507):1–12
21. Liang Z, Xing H, Wang S, Williams D, Tang C (2012) A three-dimensional numerical investigation of the fracture of rock specimens containing a pre-existing surface flaw. Comput Geotech 45:19–33
22. Litorowicz A (2006) Identification and quantification of cracks in concrete by optical fluorescent microscopy. Cem Concr Res 36(8):1508–1515
23. Liu XW, Liu QS, Liu JP, Wei L (2016) Experimental study on mechanism for fracture network initiation under complex stress conditions. Chin J Rock Mech Eng 35(S2):3662–3670
24. Lupini J, Skinner A, Vaughan P (1981) The drained residual strength of cohesive soils. Geotechnique 31(2):181–213
25. Luu VN, Murakami K, Samouh H, Maruyama I, Ohkubo T, Tom PP, Chen L, Kano S, Yang H, Abe H, Suzuki K, Suzuki M (2021) Changes in properties of alpha-quartz and feldspars under 3 MeV Si-ion irradiation. J Nucl Mater 545(152734):1–7
26. Mac MJ, Yio MHN, Desbois G, Casanova I, Wong HS, Buenfeld NR (2021) 3D imaging techniques for characterising microcracks in cement-based materials. Cem Concr Res 140(106309):1–14
27. Mandelbrot BB (1982) The fractal geometry of nature. WH freeman New York
28. Miao T, Yu B, Duan Y, Fang Q (2015) A fractal analysis of permeability for fractured rocks. Int J Heat Mass Transfer 81:75–80
29. Michie EAH, Kaminskaite I, Cooke AP, Fisher QJ, Yielding G, Tobiss SD (2021) Along-strike permeability variation in carbonate-hosted fault zones. J Struct Geol 142(104236):1–18

30. Mourzenko VV, Thovert JF, Adler PM (2011) Permeability of isotropic and anisotropic fracture networks, from the percolation threshold to very large densities. Phys Rev E 84(3):036307
31. Nikkhah AJ, Salahi E, Razavi M (2017) Application of Thermochemistry and X-ray Semi-Quantitative Phase Analysis in Forsterite Powder Synthesis by Solid State Reaction of Magnesium Oxide and Mg-Chlorite. T Indian Ceram Soc 76(3):189–195
32. Robinson P (1983) Connectivity of fracture systems-a percolation theory approach. J Phys A: Math Gen 16(3):605
33. Saevik PN, Nixon CW (2017) Inclusion of Topological Measurements into Analytic Estimates of Effective Permeability in Fractured Media. Water Resour Res 53(11):9424–9443
34. Sanderson DJ, Nixon CW (2018) Topology, connectivity and percolation in fracture networks. J Struct Geol 115:167–177
35. Valentini L, Perugini D, Poli G (2007) The 'small-world' nature of fracture/conduit networks: Possible implications for disequilibrium transport of magmas beneath mid-ocean ridges. J Volcanol Geoth Res 159(4):355–365
36. Valera M, Guo Z, Kelly P, Matz S, Cantu VA, Percus AG, Hyman JD, Srinivasan G, Viswanathan HS (2018) Machine learning for graph-based representations of three-dimensional discrete fracture networks. Comput GeoSci 22(3):695–710
37. Verberne BA, He CR, Spiers CJ (2010) Frictional properties of sedimentary rocks and natural fault gouge from the Longmen Shan fault zone, Sichuan, China. B Seismol Soc Am 100(5B):2767–2790
38. Walker RJ, Holdsworth RE, Armitage PJ, Faulkner DR (2013) Fault zone permeability structure evolution in basalts. Geology 41(1):59–62
39. Xia HC, Wu AQ, Lu B, Xu DD (2021) Influence Mechanism of Heterogeneity on Mechanical Properties of Rock Materials. J Yangtze River Sci Res Inst 38(03):103–109
40. Zhang G, Wei Z, Ferrell R (2009) Elastic modulus and hardness of muscovite and rectorite determined by nanoindentation. Appl Clay Sci 43(2):271–281
41. Zhou C, Li K, Pang X (2011) Effect of crack density and connectivity on the permeability of microcracked solids. Mech Mater 43(12):969–978

Figures

Figure 1

The location of the study area, the distribution of faults in the area, the borehole log and the core of fault rock

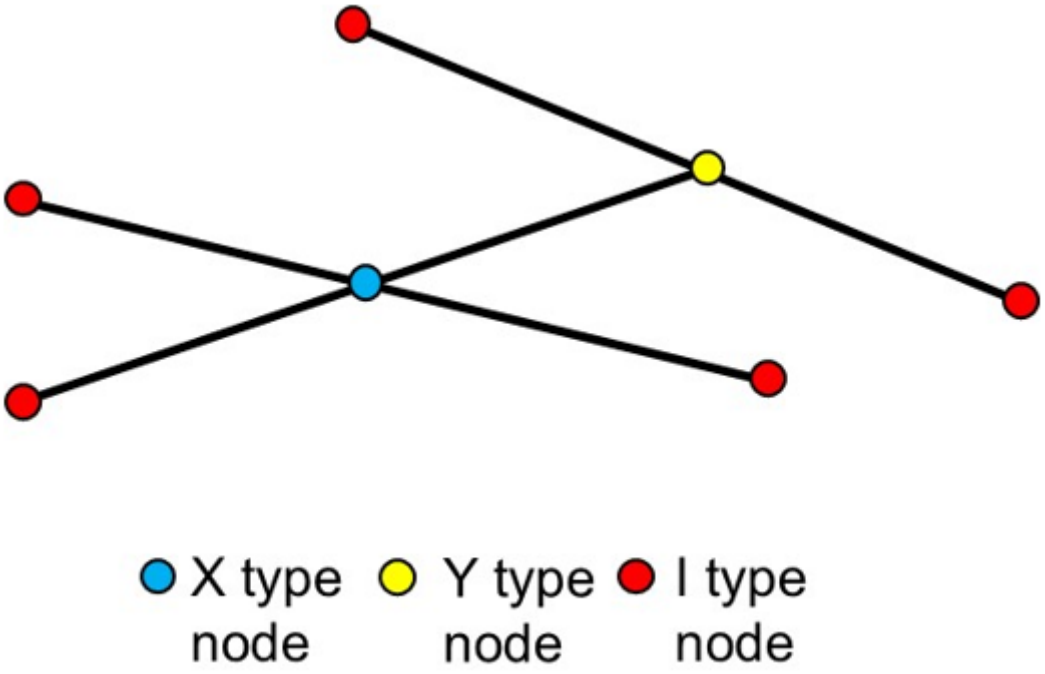

Figure 2

Topology node types

Figure 3

Optical photomicrographs (taken under plane-polarized light (PPL)) of three segments fault rock, the binary images obtained by the CAD and statistical diagram of crack length: (a) Sample depth 681.1m-681.7m, (b) Sample depth 701.6m-702.8m, (a) Sample depth 735.7m-737.3m

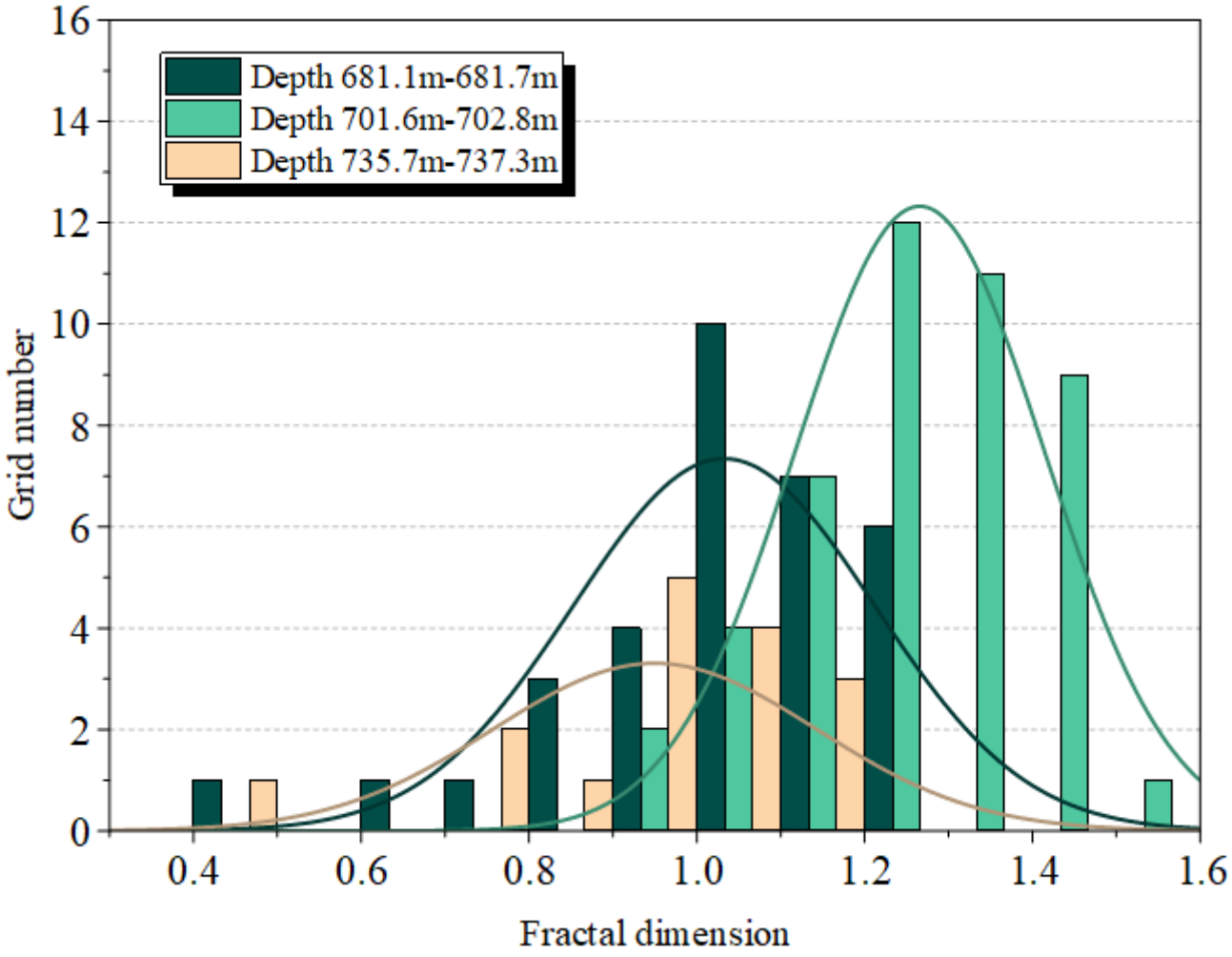

Figure 4

Fractal dimension and average value of crack network of three segment fault rocks

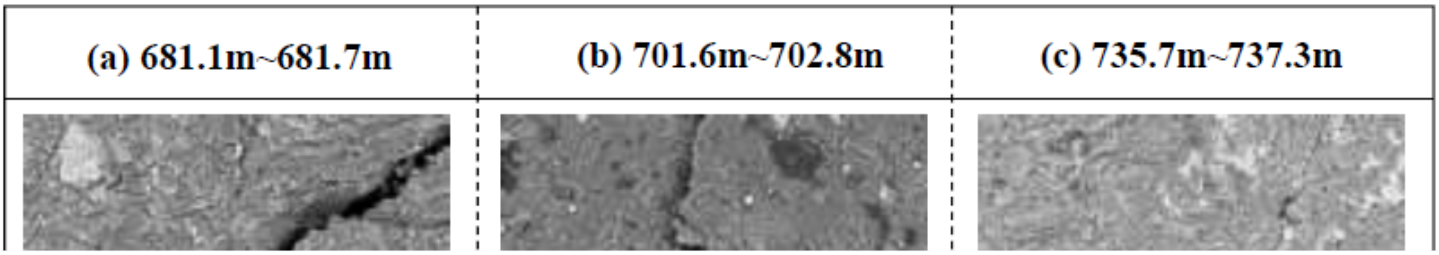

Figure 5

SEM images of three segment fault rock samples at different magnifications

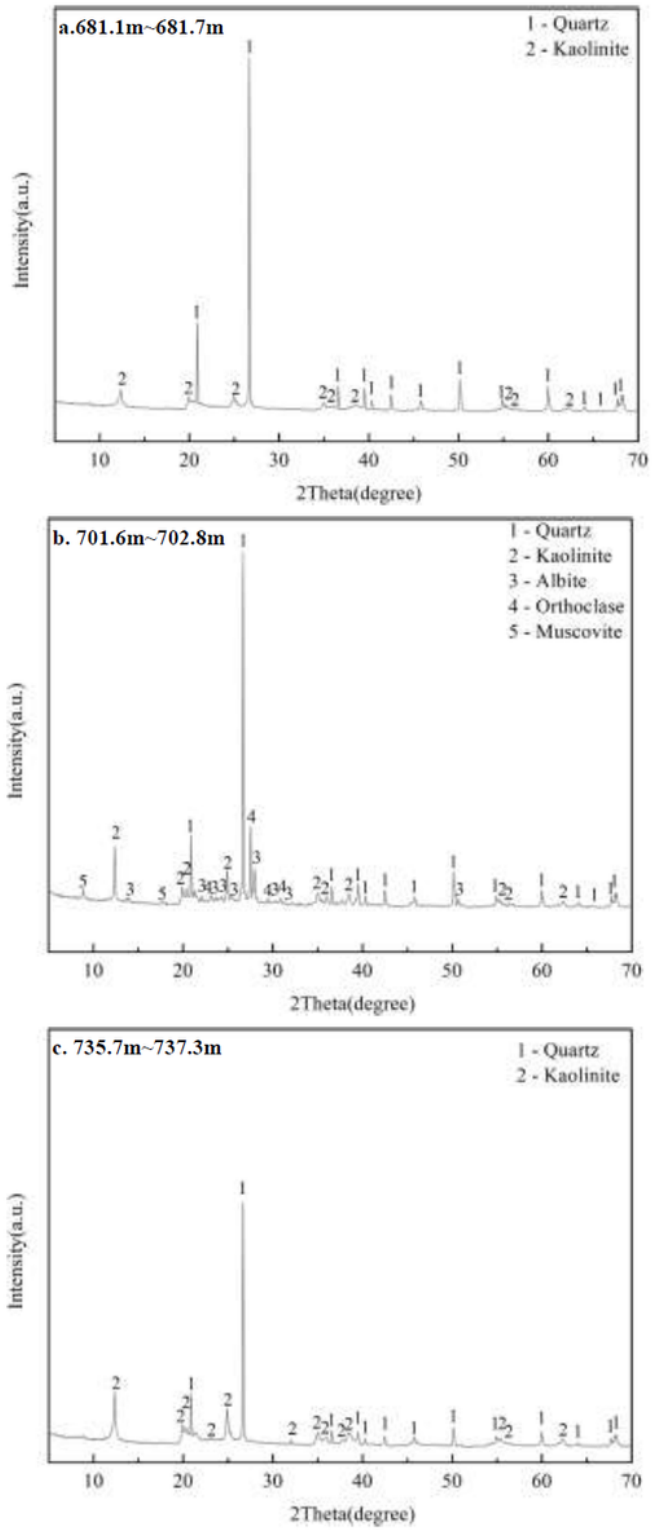

Figure 6

XRD diffraction patterns of three segment fault rocks

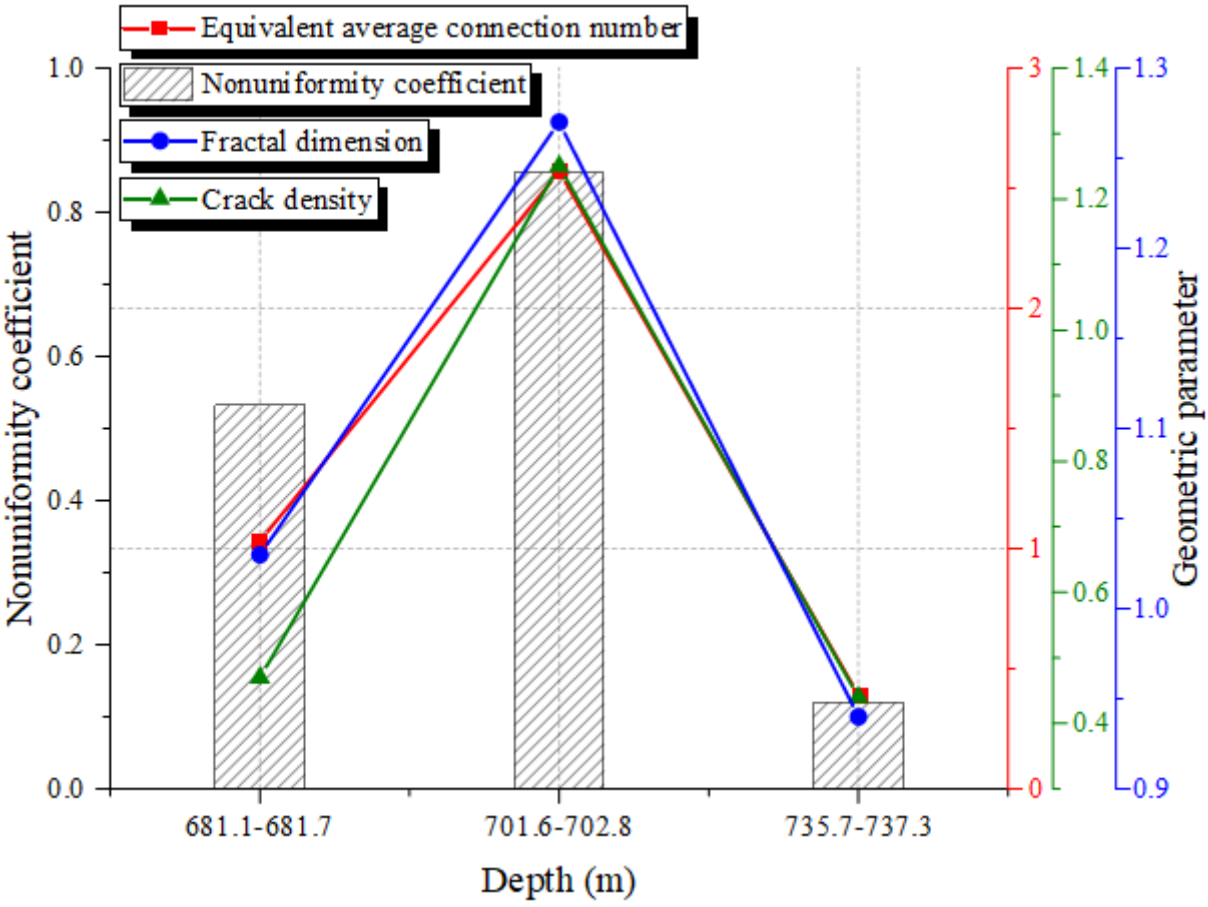

Figure 7

Nonuniformity coefficient and geometric parameters of three segment fault rock samples

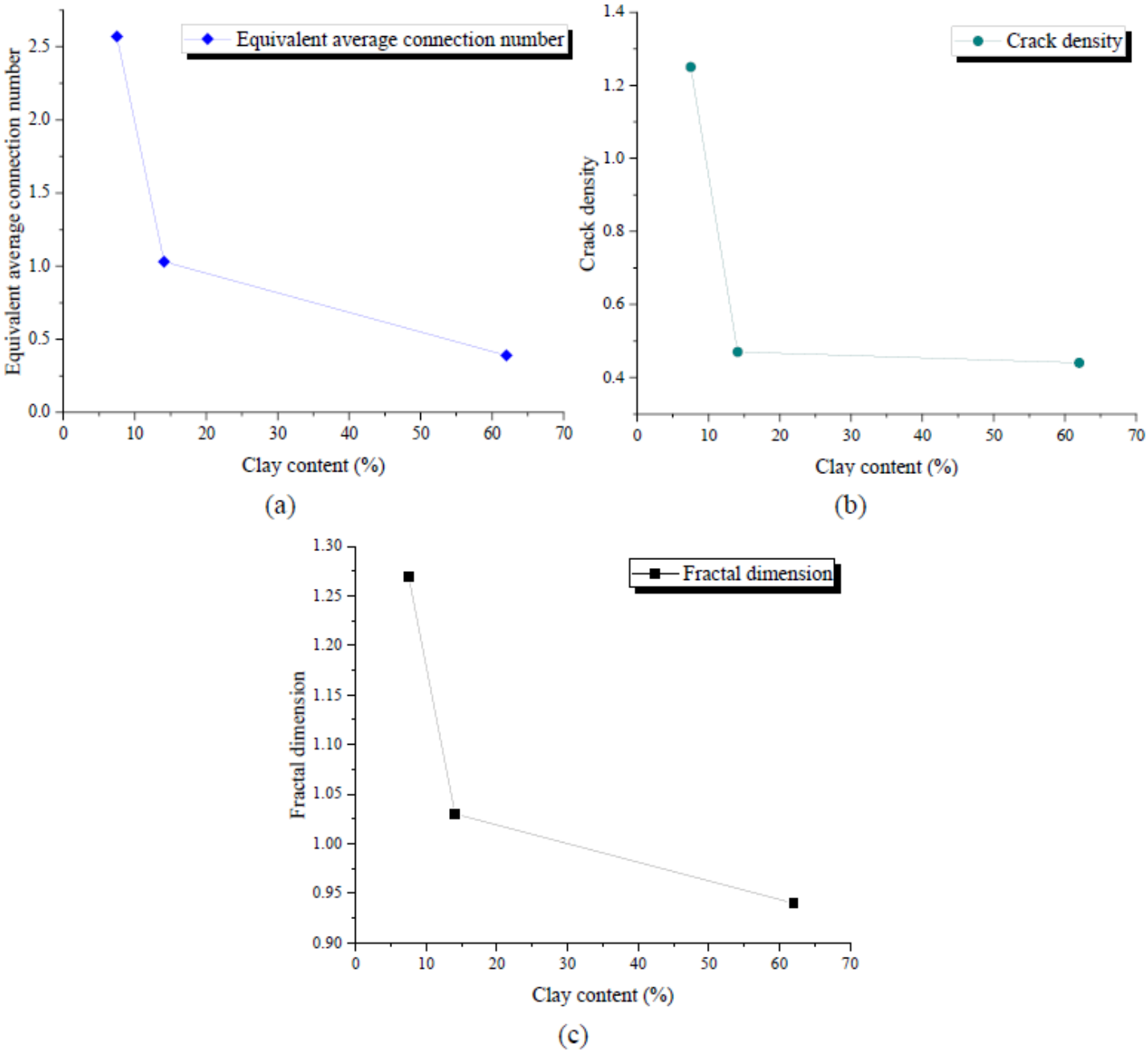

Figure 8

Variation of crack network geometric parameters of fault rock samples with kaolinite content: (a) equivalent average connection number, (b) crack density and (c) fractal dimension

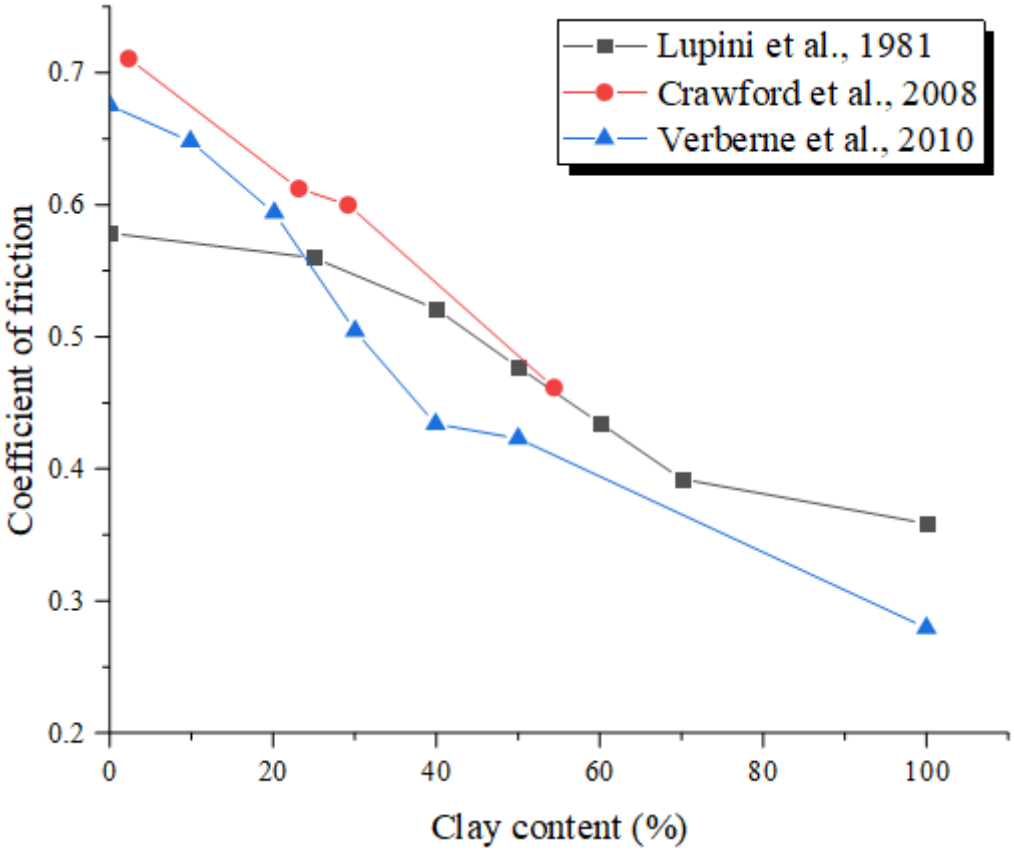

Figure 9

Coefficient of friction plotted against clay content with data from Lupini et al. (1981), Crawford et al. (2008) and Verberne et al. (2010)

Figure 10

Optical photomicrographs of fault samples: (a) one main crack (b) micro cracks which are circled in red